Bifurcation structure and chaos in dynamics of nanomagnet coupled to Josephson junction

Cite as: Chaos **32**, 093142 (2022); doi: 10.1063/5.0095009
Submitted: 7 April 2022 · Accepted: 26 August 2022 ·
Published Online: 27 September 2022

M. Nashaat,[1,2,a)] M. Sameh,[1] A. E. Botha,[3] K. V. Kulikov,[2,4] and Yu. M. Shukrinov[2,4,5]

AFFILIATIONS

[1]Department of Physics, Faculty of Science, Cairo University, 12613 Giza, Egypt
[2]BLTP, JINR, Dubna, Moscow Region 141980, Russia
[3]Department of Physics, Science Campus, University of South Africa, Johannesburg 1710, South Africa
[4]Department of Nanotechnology and New Materials, Dubna State University, Dubna, Moscow Region 141980, Russia
[5]Moscow Institute of Physics and Technology, Dolgoprudny 141700, Russia

[a)]**Author to whom correspondence should be addressed:** majed@sci.cu.edu.eg

ABSTRACT

Irregular easy axis reorientation features are observed in numerical simulations of the nanomagnet coupled to the Josephson junction. We study magnetization bifurcations and chaos that appear in this system due to the interplay of superconductivity and magnetism. The bifurcation structure of magnetization under the variation of Josephson to magnetic energy ratio as a control parameter demonstrates several precessional motions that are related to chaotic behavior and orbits with different periodicities in the ferromagnetic resonance region. The effect of an external periodic signal on the bifurcation structure is also investigated. The results demonstrate high-frequency modes of a periodic motion and a chaotic response near resonance. Far from the ferromagnetic resonance, we observe a quasiperiodic behavior. The obtained results explain the irregular reorientation of the easy axis and the transitions between different types of motion.

We present a systematic numerical study for nonlinear dynamic features in the nanomagnet coupled to the Josephson junction. Our results show that various types of magnetization dynamics of the nanomagnet may lead to fluctuations in the reorientation of the easy axis. This opens up unique perspectives for the control and manipulation of chaos in hybrid superconducting systems. In particular, we envisage that our results may be of considerable importance for the development of spintronic devices.

I. INTRODUCTION

Spintronics is currently one of the main contenders for next-generation nanoscale devices aiming at faster processing speeds and lower power consumption.[1] On the other hand, superconductors stand out as ultra-low energy dissipation systems. Superconductivity, thus, has the potential to reduce inherent heating effects in spintronic devices. As such, many different approaches have been developed to enhance spintronic effects through the incorporation of superconductivity and understand the interactions that arise due to the coexistence of superconducting and magnetic states. Such efforts have spawned the relatively new field of superconductor spintronics.[2,3] Moreover, molecular nanomagnets[4–6] are good candidates for qubit realization due to their long magnetization relaxation times.[7–10]

One of the most challenging tasks in nonlinear dynamical systems is the characterization of periodicity and chaos.[11,12] Many topological structures, e.g., shrimps, boomerangs, or both, have been observed within chaotic domains.[13–17] Since the magnetization dynamics of magnetic particles is described by the nonlinear Landau–Lifshitz–Gilbert (LLG) equation,[18] complex dynamical behaviors and bifurcations can take place for these systems also.[19–31] Recent experimental work, for example, has observed chaotic states due to driven pumping in a mono-domain regime.[32]

Chaotic behavior in the nonequilibrium dynamics of certain many-body systems can provide a way to investigate eigenstate thermalization and delocalization of such closed quantum systems. Demonstration of quantum phase transition, the onset of chaos, and the formation of many body quantum scars in the ergodic dynamics of an interacting quantum system describing a Bose–Josephson junction coupled to a single Bosonic mode was presented in Ref. 33. There, it was shown that the trajectories around the steady states

of π-mode are unstable with a positive Lyapunov exponent, which indicates a deviation from ergodicity by scarred states (deviated states) of unstable π-oscillations.

Chaos within a single driven Josephson junction (JJ) has been reported within the contexts of the resistively-capacitively shunted junction (RCSJ) and resistively-capacitively-inductively shunted (RCL-shunted) models and has also been observed experimentally.[34] Chaos is also known to occur in coupled systems of Josephson junctions. In Ref. 35, for example, the occurrence of spontaneous chaos synchronization in certain regions of the parameter space of the capacitively coupled Josephson junction with diffusion current (CCJJ+DC) model of intrinsic Josephson junctions was demonstrated, i.e., for a system without any external shunting or ac-drive. In this case, as the dc-bias current decreases along the outer resistive branch of the I-V characteristic, the system develops a break-point region, just before transition to inner branches due to the excitation of a longitudinal plasma wave. Within the break-point region, quasi-periodic and fully developed chaos can occur. More recently, chaotic behavior along the resonance circuit branch (rc-branch) of the RLC-shunted model of intrinsic Josephson junctions has also been studied.[36] In Ref. 36, the dynamics was investigated over a wide region of the parameter space through numerical simulations of the I-V characteristics, electrical charge density, Lyapunov exponents, bifurcation diagrams, and Poincaré sections. The crucial role played by the rc-frequency in determining the regions of chaos and regular behavior was demonstrated. In particular, it was found that at the lower-current end of the rc-branch, the chaotic region can be made wider (or narrower) by reducing (or increasing) the rc-frequency.

Chaotic behavior in arrays of intrinsic Josephson junctions was seen at intermediate values of coupling and dissipation parameters.[37] For specific values of dissipation and coupling parameters, the system shows instability, branching for overcritical currents appears on the I–V characteristic as well as for subcritical currents and chaotic behavior confirmed by the positive Lyapunov exponent.

In Ref. 38, the authors investigated the control of chaos and coexisting attractors and collective dynamics in a model of linear resistive-capacitive-inductive shunted Josephson junction. It was shown that the chaos in the system could be suppressed by a single feedback controller. Moreover, a linear augmentation control method can destroy the coexisting attractors between chaos and limit cycles. To understand the network behavior, the collective behavior of the system was analyzed through a two-dimensional lattice array.

Hybrid structures, such as the nanomagnet coupled to Josephson junction (NM-JJ), are important contenders for the development of spintronic devices.[39,40] In the latter structures, the dynamics of a magnetic nanoparticle and that of the JJ are governed by a nonlinear differential system of equations, which includes the LLG equation,[18] and resistively and capacitively shunted Josephson junction model.[41] The coupling in the NM-JJ system can be established in different ways, particularly, through spin–orbit coupling in the φ_0-junction.[42] Another type of coupling is realized in the NM-JJ, when electromagnetic coupling takes place between spin-waves and the Josephson phase.[43–50]

Nonlinear dynamics of the JJ is sensitive to the orientation of magnetization,[51–59] and rich physics was predicted due to this type of coupling between the Josephson and magnetic subsystems: for example, supercurrent-induced magnetization dynamics.[59–62] In the NM-JJ, the reversal of the magnetic moment by the supercurrent pulse,[57] the appearance of devil's staircase,[43] and Kapitza pendulum effects[39,63,64] were investigated.

In Refs. 39 and 63, the authors introduced the Kapitza pendulum as a mechanical analog to the NM-JJ system and demonstrated the reorientation of the easy axis of the magnetic moment of the nanomagnet. In this case, the Josephson to magnetic energy ratio G plays the role of the drive amplitude of the variable force, and the Josephson frequency Ω_J plays the role of the drive frequency in the Kapitza problem. The average magnetization component m_z characterizes the changes of the stability position. However, at present, to the best of our knowledge, there is no systematic study of the nonlinear dynamic features in the NM-JJ system. Therefore, in this paper, the dynamical equations, which describe the coupling in this system in the framework of the voltage-biased Josephson junction, are studied. We investigate magnetization bifurcations and chaos that appear in the system due to the interplay of superconductivity and magnetism and calculate the bifurcation diagrams, Lyapunov exponents, and Poincaré sections. Several precessional motions related to chaotic behavior and periodic orbits in the ferromagnetic resonance region (FMR) are demonstrated. The chaos driven by the external periodic signal is also investigated. The estimation of the model parameters shows that there is a possibility for the experimental observation of the predicted phenomenon.

The plan for the rest of the paper is as follows. In Sec. II, we describe the model and present the estimation of the model parameters. The dynamics and reorientation features of the nanomagnet coupled to Josephson junction are demonstrated in Sec. III. This is followed by a discussion of bifurcation diagrams and Poincaré sections. In Sec. IV, we discuss the chaos driven by an external periodic signal. Here also, the appearance of quasiperiodic motion is presented. Finally, we conclude with Sec. V.

II. MODEL

We consider a short Josephson junction (JJ) with length l, coupled to a single-domain nanomagnet with magnetization $\mathbf{M}$ and easy axis in the y-direction. The nanomagnet is located at a distance $r_M = a\hat{e}_x$ from the center of the junction, as shown in Fig. 1. The magnetic field of the nanomagnet alters the Josephson current, while the magnetic field generated by the Josephson junction acts on the magnetization of the nanomagnet. Thus, there is an electromagnetic interaction between the Josephson junction and the nanomagnet.

The magnetization dynamics in the NM-JJ can be described by the LLG equation,[65,66]

$$\frac{d\mathbf{M}}{dt} = -\gamma \mathbf{M} \times \mathbf{H}_{eff} + \frac{\alpha}{M_0}\left(\mathbf{M} \times \frac{d\mathbf{M}}{dt}\right), \tag{1}$$

where α is the Gilbert damping parameter and γ is the gyromagnetic factor.[11,26] The effective field in the LLG equation is given by Ref. 42,

$$H_{eff} = -\frac{1}{V_F}\frac{\partial E}{\partial M}, \tag{2}$$

where V_F is the volume of the nanomagnet, and the total energy (E) of the system is the sum of magnetic anisotropy energy (E_M), Josephson energy (E_J), and Zeeman energy (E_Z). The first two terms are

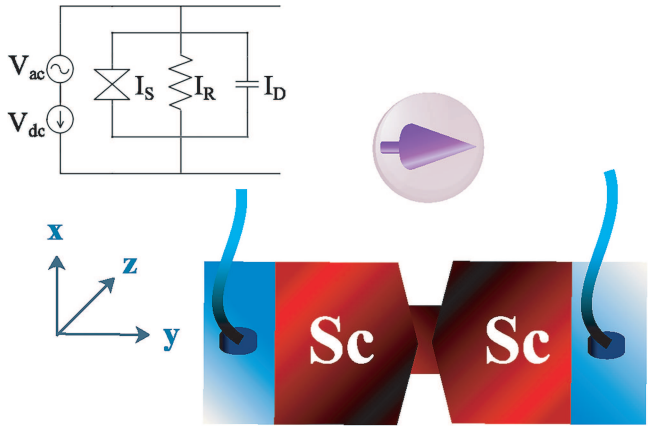

FIG. 1. Schematic diagram showing the geometry of the nanomagnet coupled to short Josephson junction (NM-JJ) studied in this work. In the equivalent circuit for the Josephson junction, V_{dc} is the bias voltage, V_{ac} is the ac external drive, I_S is the superconducting current, I_R is the resistive current, and I_D is the displacement current.

given by

$$E_M = -\frac{K_{an} V_F}{2} \left(\frac{M_y}{M_0}\right)^2, \tag{3}$$

$$E_J = \epsilon_J \left[1 - \cos\left(\frac{2\pi}{\Phi_0} V_{dc} t + \varphi_m\right)\right]. \tag{4}$$

Here, K_{an} is the magnetic anisotropy constant, $M_0 = |\mathbf{M}|$ is the saturation magnetization, $\epsilon_J = \Phi_0 I_c/2\pi$, I_c is the critical current of the JJ, Φ_0 is the flux quantum, and V_{dc} is the bias voltage for JJ. The phase shift φ_m is induced by the mutual interaction of the nanomagnet and JJ. This shift can be calculated from the vector potential $\mathbf{A}_m(\mathbf{r}, t)$, which takes into account the magnetic field of the nanomagnet created at point r and external magnetic fields, if considered (see, Refs. 40 and 63 for details). Accordingly,[40] the shift is given by

$$\varphi_m = -\frac{2\pi}{\Phi_0} \int d\boldsymbol{l} \cdot \mathbf{A}_m(\mathbf{r}, t) = -k \frac{M_z}{M_0},$$
$$\mathbf{A}_m(\mathbf{r}, t) = \frac{\mu_0}{4\pi} \frac{\mathbf{M} \times \mathbf{r}}{r^3}, \tag{5}$$
$$k = \frac{1}{2\Phi_0} \frac{\mu_0 M_0 l V_F}{a\sqrt{a^2 + l^2}},$$

where the integration goes from one side of the junction to the other, μ_0 is the permeability of free space, and k plays the role of coupling in the system.

The last term that contributes to the total energy is generated by the normal current and is given by Refs. 40 and 63,

$$E_z = -I_N \int d\boldsymbol{l} \cdot \mathbf{A}_m(\mathbf{r}, t), \tag{6}$$

where in the dimensionless form $I_N = [V - k\dot{m}_z]$, and $V = V_{dc}/I_c R$ is the normalized voltage. In our normalization, $V = \Omega_J$, $\Omega_J = \omega_J/\omega_c$, ω_J is the Josephson frequency $\omega_J = 2\pi V_{dc}/\Phi_0$, $\mathbf{m} = \mathbf{M}/M_0$, t is normalized to ω_c^{-1}, $\omega_c = 2\pi I_c R/\Phi_0$ is the Josephson characteristic frequency, R is the junction resistance, ω_F is the ferromagnetic resonance frequency, $\Omega_F = \omega_F/\omega_c$, and the effective field $\mathbf{h}_{eff}$ is normalized to the magnetic anisotropy field. According to this, the LLG equation is

$$\frac{d\mathbf{m}}{dt} = -\frac{\Omega_F}{(1+\alpha^2)} \left(\mathbf{m} \times \mathbf{h}_{eff} + \alpha \left[\mathbf{m} \times (\mathbf{m} \times \mathbf{h}_{eff})\right]\right), \tag{7}$$

with

$$h_y = m_y, \quad h_z = \epsilon[\sin(\Omega_J t - k m_z) + \Omega_J - k\dot{m}_z], \tag{8}$$

where h_y and h_z are the components of the effective field in the y- and z-direction, respectively, $\epsilon = Gk$, $G = \epsilon_J/K_{an} V_F$ is the Josephson to magnetic energy ratio, and it can be $<< 1$ or $>> 1$.[42] The first term in h_z represents the magnetic field generated by the superconducting current, while the second and third terms represent the magnetic field due to the quasiparticle current. For experimental realization of such a system, we introduce an estimation for model parameters based on Refs. 67–70. We present in Table I estimations for typical Josephson junctions, in Table II for typical nanomagnet parameters, and in Table III for model parameters. The value of k depends on the distance of the nanomagnet from the JJ and the length of the junction (here, for estimation, we consider $a = 250\,\mu$m). Experimental results give the estimation for the ferromagnetic resonance frequency of nanomagnets within ~GHz.[71,72] In the voltage-biased Josephson junction, one can tune the Josephson frequency within a wide interval around the FMR frequency.

The results presented in the paper have been obtained using different numerical methods. In particular, we solve Eq. (1) numerically using an implicit Gauss–Legendre method to calculate the dynamics of the system.[73] After allowing for a transient time, which is on the order of 10 000 dimensionless time units, we calculate the time average of magnetization components $< m_i(t) >, i = x, y, z$. To characterize different types of motions manifested in the bifurcation diagrams, we also calculate the corresponding Poincaré sections and maximal Lyapunov exponent (λ_{max}), again, after transient time.

TABLE I. Typical Josephson junction parameters.

Parameter	$Al/Al_2O_3/Al$ (SIS[a])	Nb/PdAu/Nb (SNS[b])
l (length)	141 nm	20 nm
I_c(Critical current)	20 nA	6 mA
ϵ_J (Josephson energy)	6.58×10^{-24} J	1.97×10^{-18} J
R[c] (Junction resistance)	10 kΩ	0.003 Ω
ω_c (Characteristic frequency)	~600 GHz	~54 GHz

[a]From Ref. 67.
[b]From Ref. 69.
[c]In the subgap region of voltages $V < V_g$, the junction resistance can be replaced by linear subgap resistor R_s and by the junction normal resistance R at voltages $V > V_g$, where $V_g = 2\Delta/e$ is the gap voltage and Δ is the superconducting energy gap in S-electrodes.[75] In this case, the estimation of ω_c may increase or decrease in comparison to the values in Table I.

TABLE II. Nanomagnet parameters.

Parameter	$SmCo_5$ (NM-1)	$Fe_{65}Co_{35}$ (NM-2)
M_0 (Magnetization) (kA/m)	907	1950
K_{an} (Anistropic constant) (kJ/m^3)	17 000	20
Curie temperature (K)	995	1210
V_F (Volume)	$\sim 1.979 \times 10^{-23}$ m^3	
α (Gilbert damping)	$\sim 0.0001 - 0.1$	
a (Distance of NM)	$\sim$250 nm	

Bifurcation (or orbit) diagrams are a useful tool to determine the long-term behavior and structural changes of the system's motion as one of the control parameters (in this case G, or Ω_J) are varied.[74] In this work, we use the Josephson period $\tau_J = 2\pi/\Omega_J$ as the sectional plane for constructing bifurcation diagrams such as those shown in Fig. 3. The system of equations (1) is integrated at each specific parameter value for 10 000 dimensionless time units using a fixed time step of $\Delta t = 10^{-4}$. To avoid recording any transient behavior, we only save the coordinates of the magnetization components for the last 200 "crossings," i.e., at values of time $t = p\tau_J, (p+1)\tau_J, \ldots (p+200)\tau_J$, where p is some large positive integer. When the coordinate of a particular component (say m_x) coincides for all 200 successive crossings, we have period-1 behavior in m_x, which we denoted by P1 in Fig. 3(a), for example. When there are only two distinct crossing points, we have period-2 (P2) behavior and similarly for period-3 (P3), period-4 (P4), etc. On the other hand, a continuum of points on the bifurcation diagram may reflect either quasiperiodic or chaotic behavior. To distinguish between the latter two types, we calculate the largest Lyapunov exponent λ_{max}.[20,26] When λ_{max} is zero to within a set numerical tolerance, it indicates either periodic or quasiperiodic motion. A negative λ_{max} shows that the system approaches the fixed point $m_x = m_y = 0$, $m_z = 1$, for which the time average $< m_z(t) >= 1$. A positive λ_{max} is a signature of the chaotic behavior. To find $\lambda_{\max}$ as a function of G, we first calculate the magnetic moment dynamics with the initial conditions $m = (0, 1, 0)$ and then randomly shift the initial condition by $\delta \approx 10^{-5}$. After that, we calculate $\lambda_{\max}$ from m_x, m_y, m_z and $m_x + \delta, m_y + \delta, m_z + \delta$ and average it over time.

If it not mentioned, we consider the ferromagnetic resonance frequency $\Omega_F = 1$, the coupling constant between the JJ and the nanomagnet $k = 0.05$, and the Gilbert damping parameter $\alpha = 0.1$.

TABLE III. NM-JJ parameters.

Parameter	$Al/Al_2O_3/Al$	Nb/PdAu/Nb
k (Coupling constant)		
NM-1	0.011	0.0017
NM-2	0.023	0.0037
G (Energy ratio)		
NM-1	1.9×10^{-8}	0.006
NM-2	1.6×10^{-5}	4.977

We have chosen the Josephson to magnetic energy ratio G and the Josephson frequency Ω_J as control parameters. All our calculations start with minimum value of $G = 0.01\pi$.

III. IRREGULAR REORIENTATION BEHAVIOR, BIFURCATION, AND CHAOS

As we mentioned above, in the present model, the magnetic field takes into account both the superconducting and quasiparticle currents. This leads to two different reorientation mechanisms of the nanomagnet easy axis. One mechanism is related to the magnetic field created by the quasiparticle current, while the other is related to the oscillating magnetic field generated by the superconducting current. The second mechanism reflects the Kapitza feature observed in the magnetization dynamics of the NM-JJ system[39,63] and φ_0-junction.[64]

The reorientation phenomenon is actually very complex. Here we investigate the details of the magnetic moment dynamics at different system parameters. Figure 2 shows the average magnetic moment component $< m_z(t) >$ as a function of the Josephson to magnetic energy ratio G at two values of Ω_J. One can see a linear change of the reorientation value from zero to one at $\Omega_J = 5$, where the stabilization of the magnetic moment dynamics and complete reorientation occurs ($< m_z(t) >= 1$). However, for $\Omega_J = 1$ (FMR condition), the fluctuations of $< m_z(t) >$ appear before the complete reorientation. To understand the origin of these fluctuations, we analyze the dynamics of the system in two cases, at FMR ($\Omega_J = \Omega_F$) and away from it.

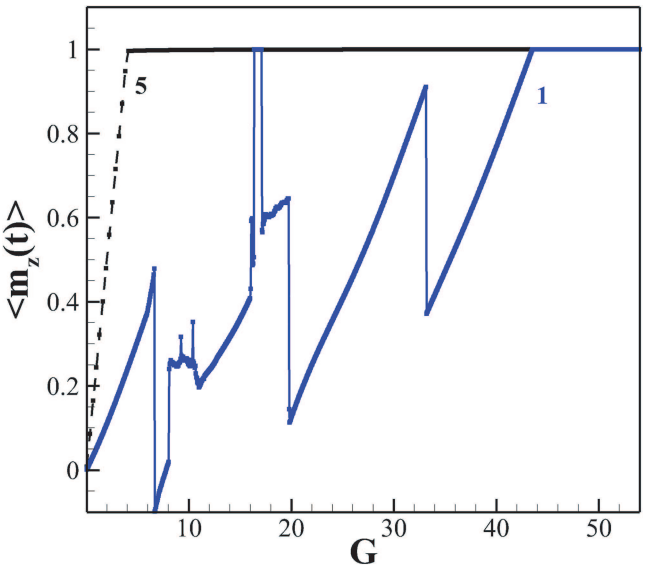

FIG. 2. The average magnetization component $< m_z(t) >$ as a function of G, demonstrating the Kapitza pendulum features in the NM-JJ system.[39,63] The blue solid line indicates the results calculated at $\Omega_J = 1$. The black dashed line shows the same at $\Omega_J = 5$.

A. Dynamical effects at FMR

To investigate the motion of the magnetic moment in the parameter space (Ω_J, G) at the FMR, we calculate the bifurcation diagrams.[26] Figures 3(a)–3(c) show the bifurcation tree of the Poincaré section of magnetization components ($m_{i\text{-Poin}}$, $i = x, y, z$) as a function of G before complete reorientation. In what follows, we describe all types of motion that are revealed in the bifurcation tree. As we can see, the bifurcation diagram starts with the fixed point (FP), $(m_{x,z} = 0, m_y = 1)$ and then demonstrates period one (P1) motion. The first period doubling occurs at $G = 6$, and the P2 motion persists up to $G < 7.9$ after which there is the second period doubling followed by P4 motion for m_x. The chaotic bands appear in the intervals $(8, 11.5)$ and $(16, 20)$, interrupted by periodic motion. In the periodic region within the intervals $(12.7, 16)$ and $(30, 43.5)$, the system demonstrates P2 motion for m_x and m_y, while m_z shows the regular P1 motion. In addition to this, two folding bifurcations are revealed [indicated by the hollow arrows in Fig. 3(a)]. Finally, the system approaches the stable fixed point (FP) at $G = 43.5$ corresponding to the complete reorientation of the easy axis $(m_{x,y} = 0, m_z = 1)$.

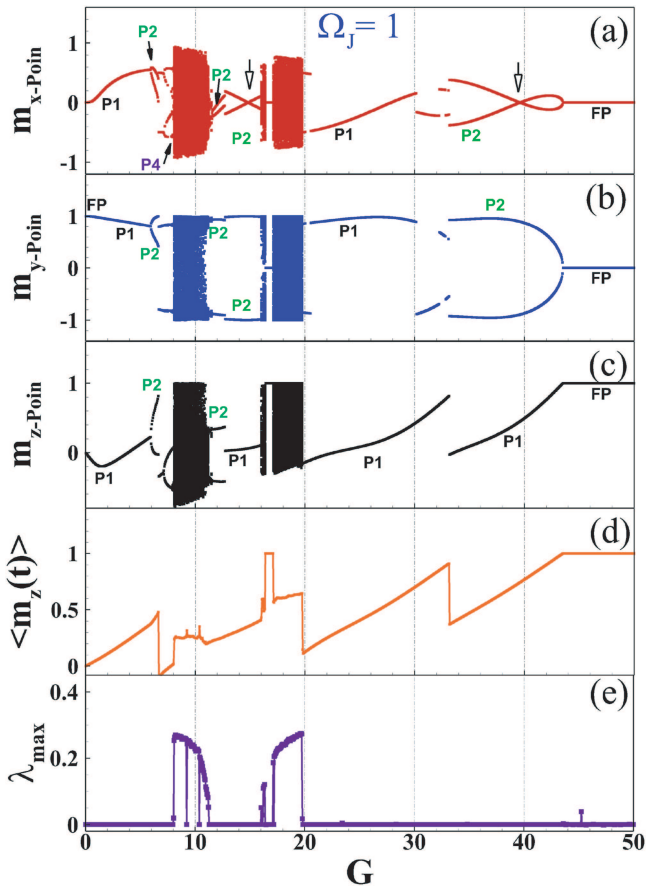

FIG. 3. Bifurcation diagrams of magnetization components (a) $m_{x\text{-Poin}}$, (b) $m_{y\text{-Poin}}$, and (c) $m_{z\text{-Poin}}$. The average value of the m_z-component is shown in (d), and (e) shows the largest Lyapunov exponent as a function of G at $\Omega_J = 1$. The folding bifurcations are indicated by hollow arrows.

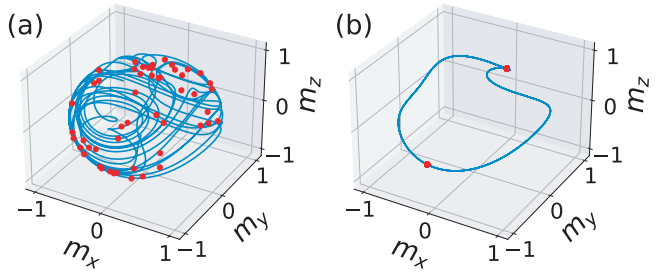

FIG. 4. The orbits of motion (blue curve) of the system and the corresponding Poincaré sections (red dots). (a) at $G = 9$ with chaos; (b) at $G = 12$ with P2 motion. Both panels are for the case with $\Omega_J = 1$. The Poincaré sections with one point only indicate P1 motion, with two points—P2 motion, and so on.

The transition from one type of motion to another, in this system, is accompanied by abrupt changes in the values of average magnetization components. We demonstrate such changes in Fig. 3(d), where the irregular reorientation behavior of $< m_z(t) >$ appears before complete reorientation. The λ_{max} calculation confirms the chaotic behavior of magnetization [see Fig. 3(e)]. The intervals with positive values of λ_{max} coincide with the chaotic bands observed in the bifurcation diagrams.

To study the dynamics of the system in more detail at specific values of G, we calculate the Poincaré sections along with the orbits of motion. These results are presented in Fig. 4. Figure 4(a) confirms the chaotic nature of those states. Figure 4(b) demonstrates the trajectories and the Poincaré section of the P2 motion at $G = 12$.

So we have demonstrated the transformations of the magnetization dynamics between different types of motion presented in the bifurcation diagrams and the Poincaré sections. These transformations lead to fluctuations in the reorientation processes of the easy axis. However, now the question arises, how the dynamics of the system changes with changing parameters.

B. Effect of Ω_J on the dynamics

The magnetic moment dynamics drastically changes at $\Omega_J > \Omega_F$ in comparison to the case $\Omega_J = \Omega_F$. Figures 5(a)–5(c) show the bifurcation trees of magnetization as a function of G at $\Omega_J = 1.5$. In this case, a simpler bifurcation structure is observed for precessional motion as compared to $\Omega_J = 1$. Chaos does not appear and the bifurcation trees at $\Omega_J = 1.5$ demonstrate motions with different periods. The λ_{max} equals zero within the whole calculation range (not shown here). The average $< m_z(t) >$ as a function of G in Fig. 5(d) reflects the transformation of the system from one kind of periodic motion to another.

Figure 6 demonstrates the corresponding shrinking of the orbits of motion with increasing of Ω_J. The increase in the driving frequency Ω_J reduces also the value of G at which the complete reorientation occurs (see the dashed line in Fig. 2).[39,63] This explains why only the P1 motion before the stable FP is observed at $\Omega_J = 5$; this is shown in Fig. 2 (dashed-line).

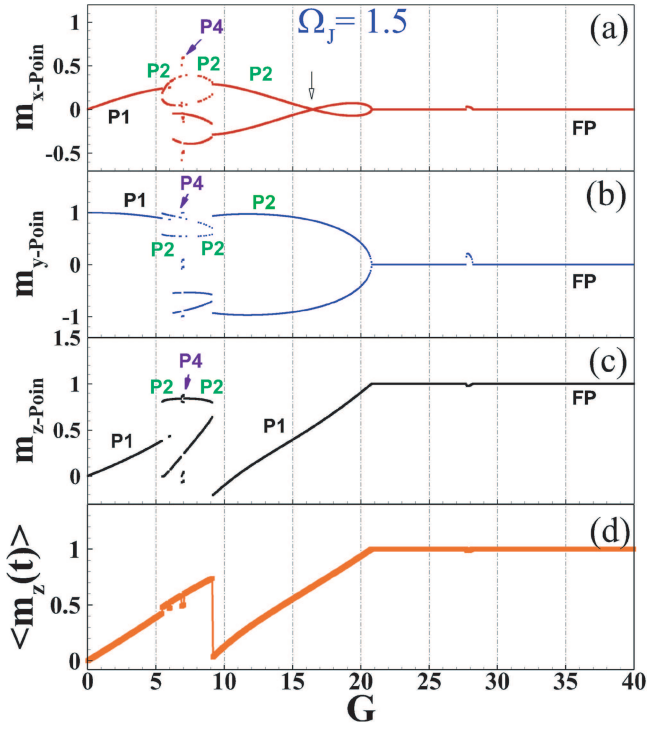

FIG. 5. Bifurcation diagram of the magnetization components (a) m_{x-Poin}, (b) m_{y-Poin}, (c) m_{z-Poin}, and (d) the average value of the m_z-component as a function of G at $\Omega_J = 1.5$. The folding bifurcation is indicated by the hollow arrow.

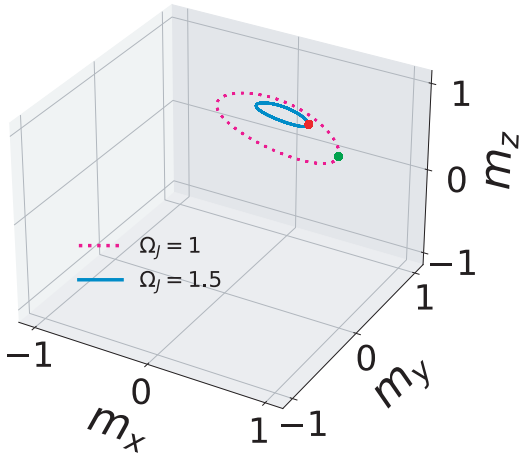

FIG. 6. The orbits of the motion of magnetization (dashed line for $\Omega_J = 1$, solid line for $\Omega_J = 1.5$) and the corresponding Poincaré sections at $G = 5$.

To determine the sensitivity of the system to different initial conditions, we calculate the basins of attraction at different values of Ω_J. In Fig. 7, we have computed the basins of attraction for $G = 10$ and two different values of Ω_J. At $\Omega_J = 1$, it shows that all possible initial conditions lead to the chaotic attractor. This is shown by the light blue color corresponding to C on the color scale. The situation changes at $\Omega_J = 1.5$ when there is no chaotic attractor. In this case, different initial conditions may lead to either P1 or P2 motion, as indicated by red and green color regions. So we have demonstrated the effect of Ω_J on bifurcation diagrams and basins of attraction, which shows the disappearance of the chaotic behavior for $\Omega_J > \Omega_F$.

C. Regions of chaos

To determine the area of chaotic response in the parameter space, we calculate 2D maps for λ_{max} as a function of G and Ω_J (see Fig. 8) at different values of k and α. In Figs. 8(a)–8(d), the λ_{max} shows only positive values for $\Omega_J < 1.5$, i.e., for $\Omega_J > 1.5$, no chaotic

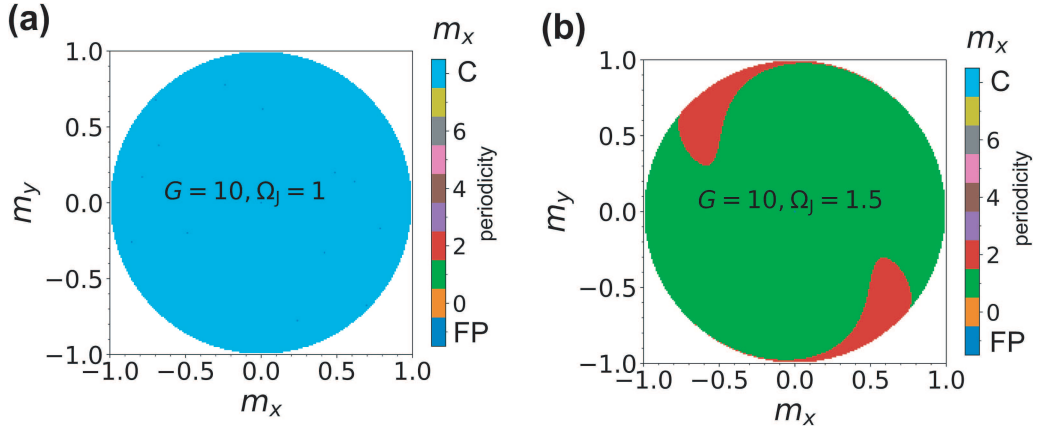

FIG. 7. Projections onto the $m_x m_y$-plane of the basins of attraction at $G = 10$ and (a) $\Omega_J = 1$, (b) $\Omega_J = 1.5$. Colors (1–7) indicate the periodicity toward which the final trajectory can be attracted, while the colors marked C corresponds to a chaotic attractor. In both figures, no FP were detected. In (a), all points are attracted to C, while in (b) the points are either attracted to period-1 (green) or period-2 (red), as indicated in the color scale (same for both figures).

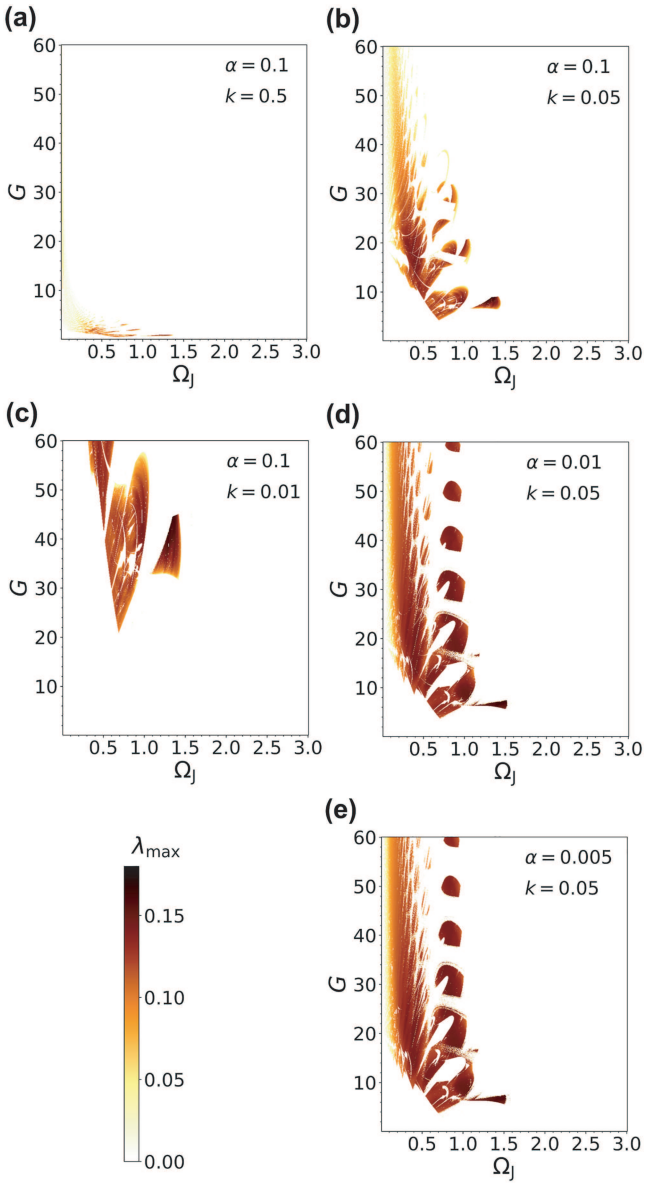

FIG. 8. The largest Lyapunov exponent as a function of G and Ω_J at different values of k and $\alpha = 0.1$ are shown in panels (a)–(c). Panels (b), (d), and (e) show the same but at different values of α and $k = 0.05$.

behavior appears. A remarkable finding is that decreasing k [cf. panels (a)–(c)] shifts up the G threshold for the chaotic motion. For example, at $k = 0.05$ [see panel (b)], the chaotic region occurs for $G > 5$, while at $k = 0.01$ [see panel (c)], it occurs only for $G > 20$. On the other hand, the chaotic response of the system is much less sensitive to changes in α, over the experimentally relevant range [cf. panels (b), (d), and (e)].

In the present system, the precession of magnetization is driven by Josephson oscillations. So the increase in Ω_J forces the magnetization to follow the Josephson oscillations, and only the periodic motion is observed. Therefore, it is the reason why we do not see any chaotic behavior of magnetization at $\Omega_J \geq 1.5$. The reorientation features at $\Omega_J >> \Omega_F$ demonstrate the Kapitza-like pendulum, as it is demonstrated in detail in Refs. 39 and 63.

In Fig. 9, we demonstrate the two-dimensional (2D) bifurcation diagrams that show the periods of magnetic moment components. Comparing with the result presented in Fig. 8(b), we find precise agreement in the predicted chaos and periodicity as a function of G and Ω_J. However, Fig. 9 shows that there are regions where the system can have different periodicities in the three magnetization components. The 2D bifurcation diagrams for m_x and m_y are exactly the same [as shown in panel (a)], while there is a remarkable difference observed for m_z [cf. panels (a) and (b)]. In particular, the large region of P2 motion shown in red in panel (a) corresponds to P2 motion in m_x. To see the regions of synchronization more clearly, we also show [panel (c)] 2D bifurcation diagrams in which all of the magnetic components have the same periodicity. The regions where the periodicity in magnetization components differ from one

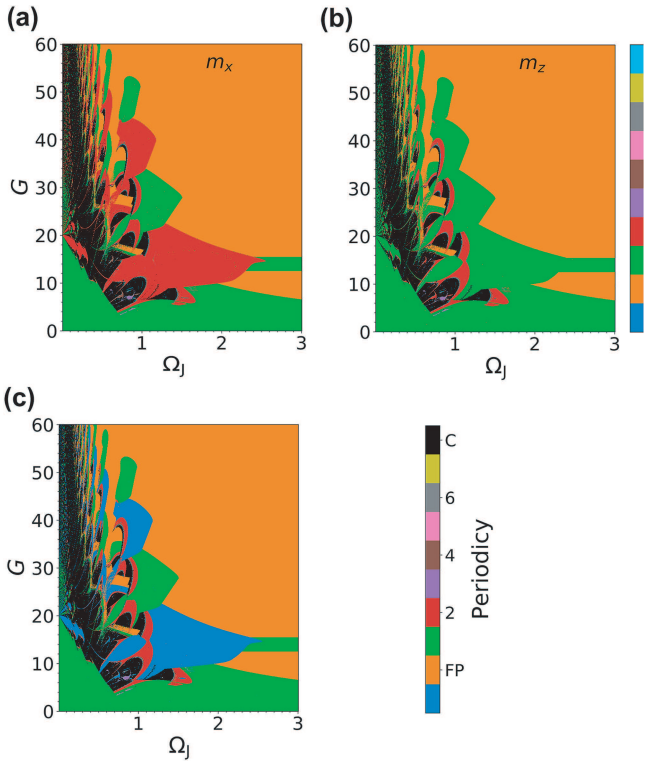

FIG. 9. Two-dimensional bifurcation diagrams over the parameter space (Ω_J, G) for (a) m_x (m_y is identical to m_x); (b) m_z; and (c) m_x, m_y, and m_z combined show the periodicity by the color scale. Orange, corresponding to 0, indicates the fixed point $m_x = m_y = 0, m_z = 1$, while in (c), the blue color corresponding to -1 indicates regions where the periodicity of the three quantities differs. The chaotic regions are colored black.

another is shown in the light blue color corresponding to minus one on the color scale. The presented diagrams show that chaos occurs only for frequencies near/or less than the FMR frequency for a wide interval of G (black color). Indeed, the chaos mostly disappears at frequency larger than the FMR frequency.

At the resolution of Fig. 9, which is 601×1201 (width $\times$ height) pixels, there appears to be some type of noise within the darker chaotic regions. However, these structures are in fact real islands of periodicity that exist within the surrounding chaotic sea. They are not related to numerical noise or artifacts. In the literature on dynamical systems, they are usually referred to as swallows or shrimps.[76–79] A discussion of their role in the chaotic dynamics would take us beyond the scope of the present work. It suffices to mention that it has recently been discussed in connection with the ordinary LLG equation (see Ref. 11).

IV. CHAOS DRIVEN BY EXTERNAL PERIODIC SIGNAL

It is well known that the external periodic signal (PS) leads to chaotic behavior in the dynamics of the SIS JJ.[80] Up to now, there has been no systematic study of the chaotic features in the NM-JJ system. Here, we demonstrate the chaotic features in the magnetization dynamics of this system under PS. The total voltage in JJ in this case consists of dc and ac parts $V_{total} = V + A\cos(\Omega_r t)$, where A is the amplitude of the PS normalized to $\hbar\omega_c/2e$ and Ω_r is the frequency of the ac voltage normalized to ω_c.

In this case, the effective field component h_z in comparison to Eq. (8) has the following form:[40,63]

$$h_z = \epsilon\left\{\sin\left(\Omega_J t - k m_z + \frac{A}{\Omega_r}\sin(\Omega_r t)\right) + \Omega_J - k\dot{m}_z + A\cos(\Omega_r t) - \beta_c A\Omega_r \sin(\Omega_r t)\right\}, \quad (9)$$

where β_c is the McCumber parameter (here we take it 0.25, which corresponds to over-damped junction) and the higher-order term $(-\beta_c k\dot{m}_z)$ is neglected, since we found from our previous estimations that $\beta_c k\dot{m}_z$ is quite small. We note that the nanomagnet effective field includes two types of oscillatory terms. One type is generated by the superconducting current with the Josepshon frequency Ω_J and amplitude proportional to G. The second type is related to the PS with frequency Ω_r and amplitude A.

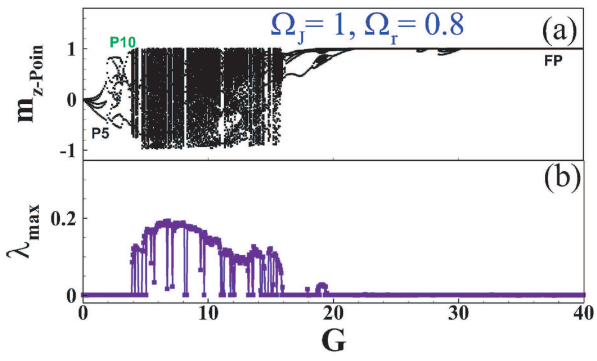

FIG. 10. (a) Bifurcation diagram of the magnetization component m_{z-Poin} and (b) the largest Lyapunov exponent as a function of G at $\Omega_J = 1$ under the external periodic signal with $\Omega_r = 0.8$ and $A = 1$.

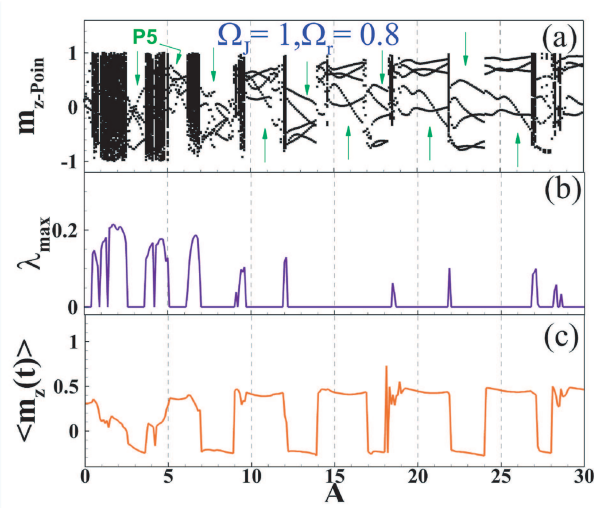

FIG. 11. (a) Bifurcation diagram of the magnetization component m_{z-Poin}, (b) the largest Lyapunov exponent, and (c) average value of the m_z-component as a function of A at $\Omega_r = 0.8$, $\Omega_J = 1$, and $G = 5$.

A. Bifurcation structure as a function of G

First, we investigate the effect of G on the bifurcation structure of the magnetization components under external PS. Figure 10 shows the bifurcation diagram of the magnetization dynamics and

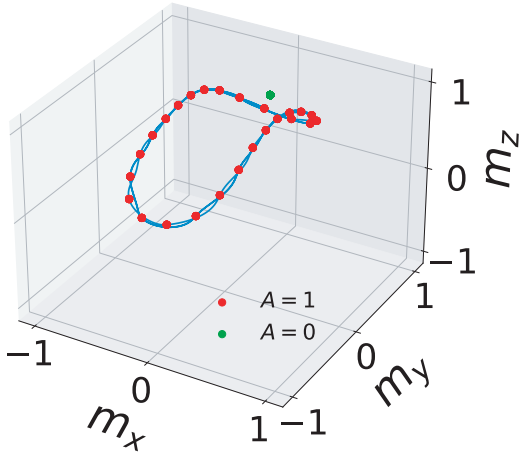

FIG. 12. The Poincaré section (green dot) with P1 motion at $A = 0$ together with the quasiperiodic orbit (blue curve) and the corresponding Poincaré section (red dots) at $\Omega_r = 0.8$, $A = 1$. Both cases are calculated at $\Omega_J = 5$ and $G = 3$.

λ_{max} at $\Omega_J = 1$, $\Omega_r = 0.8$, and $A = 1$. The bifurcation starts with P5 motion [see Fig. 10(a)]. Then, the chaotic band is observed together with very narrow windows of the periodic motion in the interval (3.8, 16), where the λ_{max} values are of the order 10^{-1} [see Fig. 10(b)].

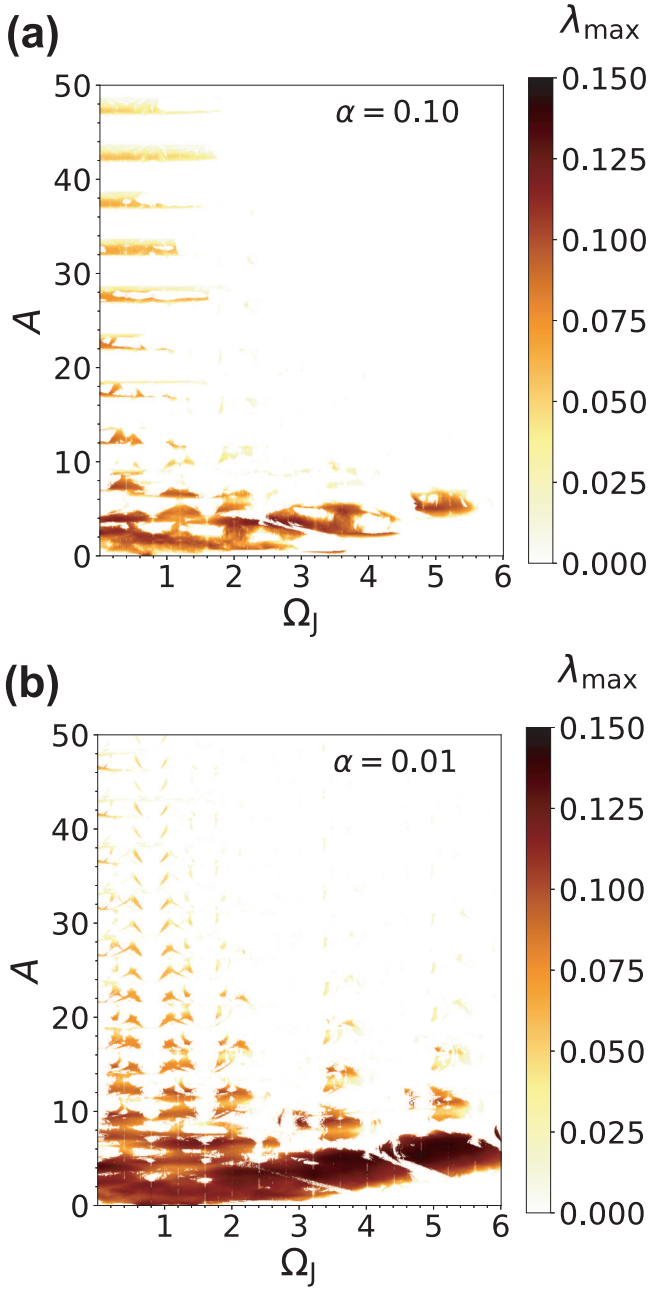

FIG. 13. (a) Maximal Lyapunov exponent as a function of A and Ω_J at (a) $\alpha = 0.1$ and (b) $\alpha = 0.01$. Other parameters are as follows: $G = 5$, $k = 0.05$, $\beta_c = 0.25$, $\Omega_F = 1$, and $\Omega_r = 0.8$.

Those windows can be distinguished as the corresponding dips on λ_{max} within the interval (4, 16).

The magnetization dynamics approaches FP at $G \geq 21.7$. Then, a small region of the periodic motion with high-order modes (P10) appears in the interval (25.3, 30.5). After that, the trajectory finds a stable FP corresponding to a complete reorientation of the magnetization direction ($< m_z(t) >= 1$). So the external periodic signal leads to a higher order periodic motion in the system.

B. Bifurcation structure as a function of A

Significant changes in the bifurcation structure can be seen with increasing amplitude A of external PS, which are shown in Fig. 11(a) for z-component (x,y components are qualitatively the same). The figure demonstrates that with slight changes in A, the system behavior transforms from P1 motion into the higher order periodic motion (for given simulation parameters, we have P5 motion) and then into chaos. At $A > 7$, the system demonstrates windows of P5 periodic motion (marked by green arrows). The transitions between those states are manifested in λ_{max} [see Fig. 11(b)], where the positive values indicate a strong chaotic response. We also note that the increase in A changes the reorientation value, as it was discussed in Ref. 63. However, at given simulation parameters, a complete reorientation of the easy axis does not occur [see Fig. 11(c)]. So by changing the amplitude of the external PS, one can transform the dynamics from the chaotic region to the periodic one. Therefore, we propose a method to control the chaotic behavior in the magnetization dynamics and reorientation process of the easy axis in the NM-JJ system by applying PS with a specific amplitude and Ω_r.

The NM-JJ system under the external PS reveals another interesting long-term behavior far from the FMR region, namely, the quasiperiodicity that mostly appears in the weak coupling regime (at small G).

In this case, the trajectories will never close onto themselves. Figure 12 demonstrates the transformation of the trajectory from P1 motion (green dot) to the quasiperiodic one (blue curve with red dots) under the influence of PS at $G = 3$ and $\Omega_J = 5$.

Finally, in Fig. 13, we determine λ_{max} over the two-dimensional parameter space, A–Ω_J. We can see that the system undergoes chaotic behavior even for $\Omega_J > \Omega_F$. For $A > 10$, the maximal exponent is positive only for frequencies near the FMR. Therefore, chaotic behavior in this system can be controlled by applying the external periodic signal as a form of chaos control.[81]

V. SUMMARY AND CONCLUSIONS

A detailed overview of various types of magnetization dynamics possible in the nanomagnet coupled to the Josephson junction has been provided. The fluctuations in the reorientation of the easy axis caused by transformations between the different types of motions of the system were demonstrated. The analysis of the bifurcation diagrams revealed the exact regions where the magnetization exhibits such motions. Chaotic states and orbits with different periodicities were found in the ferromagnetic resonance region. On the other hand, when the Josephson frequency was larger than the resonance frequency, the chaotic behavior disappeared, leaving only

periodic orbits. We found that an increase in the Josephson frequency reduces the spacial extent of the magnetization trajectory. A detailed two-dimensional picture of the maximal Lyapunov exponent over the A–Ω_J parameter showed that the application of an external periodic perturbation could help to avoid chaotic behavior in practical realizations of this system.

With the applied periodic signal, the system shows an increase in the chaotic response and the high-order modes of periodic motion intervals near the resonance. Long-term quasiperiodic behavior in the magnetization dynamics far from the resonance was also observed. In addition to this, the amplitude of the external periodic signal also affects the fact whether or not the system behaves chaotically. Therefore, one can control the chaotic behavior of the system by applying an external periodic signal of right frequency and amplitude. Given that it is difficult to adjust the magnetic energy ratio (G) for any given material, chaos control via externally applied electromagnetic radiation provides a viable practical way of suppressing unwanted chaotic behavior in this system.

We have emphasized that the system of nanomagnet coupled to the Josephson junction evinced nonlinear and chaotic phenomena, where a small quantitative change in the system parameters caused a huge qualitative change in its response. As such, the system we have studied could be used as a prototype for "tipping" behavior,[82] well known in the context of complex systems. Our findings can also be extended to other systems of superconductor spintronics like φ_0-junction, which has the same current-phase relation. Nevertheless, there are still many open questions concerning the chaos in the Josephson junction with magnetic materials. One of them is why chaotic behavior is seen in certain areas of parameters space and not others. We, thus, hope that our study will facilitate new experimental and theoretical research in this field. In particular, we envisage that it may be of considerable importance for experimental investigations of resonance and development of superconductor spintronics devices.

ACKNOWLEDGMENTS

The authors are grateful to I. R. Rahmonov and A. A. Mazanik for fruitful discussion about the results of this paper. The study was carried out within the framework of the ASRT (Egypt)-JINR (Russia) research projects. Numerical simulations were funded by Project No. 22-71-10022 of the Russian Scientific Fund. Special thanks to Bibliotheca Alexandrina supercomputing facility (Egypt), HybriLIT heterogeneous computing platform (LIT, JINR-Russia), and the high-performance computing (HPC) facility at the University of South Africa.

AUTHOR DECLARATIONS

Conflict of Interest

The authors have no conflicts to disclose.

Author Contributions

M. Nashaat: Conceptualization (lead); Data curation (equal); Investigation (equal); Methodology (lead); Software (equal); Visualization (equal); Writing – original draft (lead); Writing – review & editing (equal). **M. Sameh:** Data curation (equal); Investigation (equal); Software (equal); Visualization (equal); Writing – original draft (equal); Writing – review & editing (equal). **A. E. Botha:** Data curation (equal); Investigation (lead); Methodology (lead); Software (lead); Visualization (equal); Writing – review & editing (equal). **K. V. Kulikov:** Conceptualization (supporting); Investigation (supporting); Software (supporting); Visualization (supporting); Writing – review & editing (equal). **Yu. M. Shukrinov:** Conceptualization (equal); Methodology (equal); Software (equal); Supervision (lead); Validation (lead); Visualization (equal); Writing – review & editing (lead).

DATA AVAILABILITY

The data that support the findings of this study are available from the corresponding author upon reasonable request.

REFERENCES

[1] A. Hirohata, K. Yamada, Y. Nakatani, I. L. Prejbeanu, B. Diény, P. Pirro, and B. Hillebrands, "Review on spintronics: Principles and device applications," J. Magn. Magn. Mater. **509**, 166711 (2020).
[2] A. Golubov and M. Yu. Kupriyanov, "Controlling magnetism," Nat. Mater. **16**, 156 (2017).
[3] J. Linder and J. W. A. Robinson, "Superconducting spintronics," Nat. Phys. **11**, 307 (2015).
[4] A. Candini, S. Klyatskaya, M. Ruben, W. Wernsdorfer, and M. Affronte, "Graphene spintronic devices with molecular nanomagnets," Nano Lett. **11**(7), 2634 (2011).
[5] L. Bogani and W. Wernsdorfer, "Molecular spintronics using single-molecule magnets," Nat. Mater. **7**, 179 (2008).
[6] A. R. Rocha, V. M. García-Suárez, S. W. Bailey, C. J. Lambert, J. Ferrer, and S. Sanvito, "Towards molecular spintronics," Nat. Mater. **4**, 335 (2005).
[7] A. Chiesa, E. Macaluso, F. Petiziol, S. Wimberger, P. Santini, and S. Carretta, "Molecular nanomagnets as Qubits with embedded quantum-error correction," J. Phys. Chem. Lett. **11**, 8610–8615 (2020).
[8] R. Ghosh, M. Maiti, Yu. M. Shukrinov, and K. Sengupta, "Magnetization-induced dynamics of a Josephson junction coupled to a nanomagnet," Phys. Rev. B **96**, 174517 (2017).
[9] G. A. Cirillo, G. Turvani, and M. Graziano, "A quantum computation model for molecular nanomagnets," IEEE Trans. Nanotechnol. **18**, 1027–1039 (2019).
[10] A. Ardavan, O. Rival, J. J. L. Morton, S. J. Blundell, A. M. Tyryshkin, G. A. Timco, and R. E. P. Winpenny, "Will spin-relaxation times in molecular magnets permit quantum information processing?," Phys. Rev. Lett. **98**, 057201 (2007).
[11] J. A. Vélez, J. Bragard, L. M. Pérez, A. M. Cabanas, O. J. Suarez, D. Laroze, and H. L. Mancini, "Periodicity characterization of the nonlinear magnetization dynamics," Chaos **30**, 093112 (2020).
[12] S. Boccaletti, C. Grebogi, Y. C. Lai, H. Mancini, and D. Maza, "The control of chaos: Theory and applications," Phys. Rep. **329**, 103 (2000).
[13] R. Barrio, M. Á. Martínez, S. Serrano, and D. Wilczak, "When chaos meets hyperchaos: 4D Rössler model," Phys. Lett. A **379**, 2300 (2015).
[14] L. M. Pérez, J. Bragard, H. L. Mancini, J. A. C. Gallas, A. M. Cabanas, O. J. Suarez, and D. Laroze, "Effect of anisotropies on the magnetization dynamics," Networks Heterogen. Media **10**, 209 (2015).
[15] T. Xing, R. Barrio, and A. Shilnikov, "Symbolic quest into homoclinic chaos," Int. J. Bifurc. Chaos **24**, 1440004 (2014).
[16] W. Façanha, B. Oldeman, and L. Glass, "Bifurcation structures in two-dimensional maps: The endoskeletons of shrimps," Phys. Lett. A **377**, 1264 (2013).
[17] R. Barrio, F. Blesa, and S. Serrano, "Topological changes in periodicity hubs of dissipative systems," Phys. Rev. Lett. **108**, 214102 (2012).
[18] M. Lakshmanan, "The fascinating world of the Landau–Lifshitz–Gilbert equation: An overview," Philos. Trans. R. Soc. A **369**, 1280–1300 (2011).

[19]C. Gibson, S. Bildstein, J. A. L. Hartman, and M. Grabowski, "Nonlinear resonances and transitions to chaotic dynamics of a driven magnetic moment," J. Magn. Magn. Mater. **501**, 166352 (2020).
[20]T. Taniguchi, N. Akashi, H. Notsu, M. Kimura, H. Tsukahara, and K. Nakajima, "Chaos in nanomagnet via feedback current," Phys. Rev. B **100**, 174425 (2019).
[21]A. M. Ferona and R. E. Camley, "Nonlinear power-dependent effects in exchange-coupled magnetic bilayers," Phys. Rev. B **99**, 064405 (2019).
[22]J. Williame, A. D. Accioly, D. Rontani, M. Sciamanna, and J.-V. Kim, "Chaotic dynamics in a macrospin spin-torque nano-oscillator with delayed feedback," Appl. Phys. Lett. **114**, 232405 (2019).
[23]G. Okano and Y. Nozaki, "Evaluation of the effective potential barrier height in nonlinear magnetization dynamics excited by ac magnetic field," Phys. Rev. B **97**, 014435 (2018).
[24]A. M. Cabanas, L. M. Pérez, and D. Laroze, "Strange non-chaotic attractors in spin valve systems," J. Magn. Magn. Mater. **460**, 320 (2018).
[25]J. Hizanidis, N. Lazarides, and G. P. Tsironis, "Flux bias-controlled chaos and extreme multistability in SQUID oscillators," Chaos **28**, 063117 (2018).
[26]A. M. Ferona and R. E. Camley, "Nonlinear and chaotic magnetization dynamics near bifurcations of the Landau-Lifshitz-Gilbert equation," Phys. Rev. B **95**, 104421 (2017).
[27]S. I. Denisov, T. V. Lyutyy, B. O. Pedchenko, and O. M. Hryshko, "Induced magnetization and power loss for a periodically driven system of ferromagnetic nanoparticles with randomly oriented easy axes," Phys. Rev. B **94**, 024406 (2016).
[28]M. G. Phelps, K. L. Livesey, A. M. Ferona, and R. E. Camley, "Tunable transient decay times in nonlinear systems: Application to magnetic precession," Europhys. Lett. **109**, 37007 (2015).
[29]D. Urzagasti, D. Becerra-Alonso, L. M. Pérez, H. L. Mancini, and D. Laroze, "Hyper-chaotic magnetisation dynamics of two interacting dipoles," J. Low Temp. Phys. **181**, 211 (2015).
[30]Y. Khivintsev, B. Kuanr, T. J. Fal, M. Haftel, R. E. Camley, Z. Celinski, and D. L. Mills, "Nonlinear ferromagnetic resonance in permalloy films: A nonmonotonic power-dependent frequency shift," Phys. Rev. B **81**, 054436 (2010).
[31]L. F. Álvarez, O. Pla, and O. Chubykalo, "Quasiperiodicity, bistability, and chaos in the Landau-Lifshitz equation," Phys. Rev. B **61**, 11613 (2000).
[32]E. A. Montoya, S. Perna, Y.-J. Chen, J. A. Katine, M. d'Aquino, C. Serpico, and I. N. Krivorotov, "Magnetization reversal driven by low dimensional chaos in a nanoscale ferromagnet," Nat. Commun. **10**, 543 (2019).
[33]S. Sinha and S. Sinha, "Chaos and quantum scars in Bose-Josephson junction coupled to a bosonic mode," Phys. Rev. Lett. **125**, 134101 (2020).
[34]C. B. Whan and C. J. Lobb, "Complex dynamical behavior in RCL-shunted Josephson tunnel junctions," Phys. Rev. E **53**, 405 (1996).
[35]A. E. Botha, I. R. Rahmonov, and Yu. M. Shukrinov, "Spontaneous and controlled chaos synchronization in intrinsic Josephson junctions," IEEE Trans. Appl. Supercond. **28**, 1 (2018).
[36]A. E. Botha, Yu. M. Shukrinov, and J. Tekić, "Chaos along the rc-branch of RLC-shunted intrinsic Josephson junctions," Chaos Solitons Fractals **156**, 111865 (2022).
[37]M. Cuzminschi and A. Zubarev, "Chaotic behavior of a stack of intrinsic Josephson junctions at the transition to branching for overcritical currents," Chin. J. Phys. **71**, 634 (2021).
[38]B. Ramakrishnan, L. M. A. Tabejieu, I. K. Ngongiah, S. T. Kingni, R. T. Siewe, and K. Rajagopal, "Suppressing chaos in Josephson junction model with coexisting attractors and investigating its collective behavior in a network," J. Supercond. Novel Magn. **34**, 2761 (2021).
[39]Yu. M. Shukrinov, M. Nashaat, I. R. Rahmonov, and K. V. Kulikov, "Ferromagnetic resonance and the dynamics of the magnetic moment in a 'Josephson junction–nanomagnet' system," JETP Lett. **110**, 160 (2019).
[40]L. Cai and E. M. Chudnovsky, "Interaction of a nanomagnet with a weak superconducting link," Phys. Rev. B **82**, 104429 (2010).
[41]W. Buckel and R. Kleiner, *Superconductivity: Fundamentals and Applications* (Wiley-VCH, Berlin, 2004).
[42]A. Buzdin, "Direct coupling between magnetism and superconducting current in the Josephson φ_0 junction," Phys. Rev. Lett. **101**, 107005 (2008).
[43]M. Nashaat, A. E. Botha, and Yu. M. Shukrinov, "Devil's staircases in the IV characteristics of superconductor/ferromagnet/superconductor Josephson junctions," Phys. Rev. B **97**, 224514 (2018).
[44]S. Hikino, M. Mori, S. Takahashi, and S. Maekawa, "Microwave-induced supercurrent in a ferromagnetic Josephson junction," Supercond. Sci. Technol. **24**, 024008 (2011).
[45]S. Mai, E. Kandelaki, A. F. Volkov, and K. B. Efetov, "Interaction of Josephson and magnetic oscillations in Josephson tunnel junctions with a ferromagnetic layer," Phys. Rev. B **84**, 144519 (2011).
[46]G. Wild, C. Probst, A. Marx, and R. Gross, "Josephson coupling and Fiske dynamics in ferromagnetic tunnel junctions," Eur. Phys. J. B **78**, 509 (2010).
[47]M. Kemmler, M. Weides, M. Weiler, M. Opel, S. T. B. Goennenwein, A. S. Vasenko, A. A. Golubov, H. Kohlstedt, D. Koelle, R. Kleiner, and E. Goldobin, "Magnetic interference patterns in $0-\pi$ superconductor/insulator/ferromagnet/superconductor Josephson junctions: Effects of asymmetry between 0 and 0π regions," Phys. Rev. B **81**, 054522 (2010).
[48]A. F. Volkov and K. B. Efetov, "Hybridization of spin and plasma waves in Josephson tunnel junctions containing a ferromagnetic layer," Phys. Rev. Lett. **103**, 037003 (2009).
[49]J. Pfeiffer, M. Kemmler, D. Koelle, R. Kleiner, E. Goldobin, M. Weides, A. K. Feofanov, J. Lisenfeld, and A. V. Ustinov, "Static and dynamic properties of 0, π, and $0-\pi$ ferromagnetic Josephson tunnel junctions," Phys. Rev. B **77**, 214506 (2008).
[50]M. Weides, M. Kemmler, H. Kohlstedt, R. Waser, D. Koelle, R. Kleiner, and E. Goldobin, "$0-\pi$ Josephson tunnel junctions with ferromagnetic barrier," Phys. Rev. Lett. **97**, 247001 (2006).
[51]I. V. Bobkova, A. M. Bobkov, and M. A. Silaev, "Magnetoelectric effects in Josephson junctions," J. Phys.: Condens. Matter **34**, 353001 (2022).
[52]S. A. Abdelmoneim, Yu. M. Shukrinov, K. V. Kulikov, H. El Samman, and M. Nashaat, "Locking of magnetization and Josephson oscillations at ferromagnetic resonance in φ_0 junction under external radiation," Phys. Rev. B **106**, 014505 (2022).
[53]M. Nashaat, I. V. Bobkova, A. M. Bobkov, Yu. M. Shukrinov, I. R. Rahmonov, and K. Sengupta, "Electrical control of magnetization in superconductor/ferromagnet/superconductor junctions on a three-dimensional topological insulator," Phys. Rev. B **100**, 054506 (2019).
[54]D. S. Rabinovich, I. V. Bobkova, A. M. Bobkov, and M. A. Silaev, "Chirality selective spin interactions mediated by the moving superconducting condensate," Phys. Rev. B **98**, 184511 (2018).
[55]M. A. Silaev, I. V. Tokatly, and F. S. Bergeret, "Anomalous current in diffusive ferromagnetic Josephson junctions," Phys. Rev. B **95**, 184508 (2017).
[56]I. V. Bobkova, A. M. Bobkov, and M. A. Silaev, "Gauge theory of the long-range proximity effect and spontaneous currents in superconducting heterostructures with strong ferromagnets," Phys. Rev. B **96**, 094506 (2017).
[57]Yu. M. Shukrinov, I. R. Rahmonov, K. Sengupta, and A. Buzdin, "Magnetization reversal by superconducting current in φ_0 Josephson junctions," Appl. Phys. Lett. **110**, 182407 (2017).
[58]S. Mironov and A. Buzdin, "Triplet proximity effect in superconducting heterostructures with a half-metallic layer," Phys. Rev. B **92**, 184506 (2015).
[59]A. I. Buzdin, "Proximity effects in superconductor-ferromagnet heterostructures," Rev. Mod. Phys. **77**, 935 (2005).
[60]Yu. M. Shukrinov, "Anomalous Josephson effect," Phys.-Usp. **65**, 317 (2022).
[61]J. Linder and K. Halterman, "Superconducting spintronics with magnetic domain walls," Phys. Rev. B **90**, 104502 (2014).
[62]A. A. Golubov, M. Yu. Kupriyanov, and E. Ilichev, "The current-phase relation in Josephson junctions," Rev. Mod. Phys. **76**, 411 (2004).
[63]K. V. Kulikov, D. V. Anghel, A. T. Preda, M. Nashaat, M. Sameh, and Yu. M. Shukrinov, "Kapitza pendulum effects in a Josephson junction coupled to a nanomagnet under external periodic drive," Phys. Rev. B **105**, 094421 (2022).
[64]Yu. M. Shukrinov, A. Mazanik, I. R. Rahmonov, A. E. Botha, and A. Buzdin, "Re-orientation of the easy axis in φ_0-junction," Europhys. Lett. **122**(3), 37001 (2018).
[65]T. L. Gilbert, "A phenomenological theory of damping in ferromagnetic materials," IEEE Trans. Magn. **40**, 3443 (2004).
[66]L. D. Landau and E. Lifshitz, "On the theory of the dispersion of magnetic permeability in ferromagnetic bodies," Phys. Z. Sowjetunion **8**, 153 (1935).
[67]P. Mangin and R. Kahn, *Superconductivity: An Introduction*, 3rd ed. (Springer, Grenoble, 2016).

[68]L. F. Yin, "Magnetocrystalline anisotropy in permalloy revisited," Phys. Rev. Lett. **97**, 067203 (2006).
[69]K. H. J. Buschow, *Concise Encyclopedia of Magnetic and Superconducting Materials*, 2nd ed. (Elsevier, Amsterdam, 2005).
[70]R. P. Cowburn, A. O. Adeyeye, and M. E. Welland, "Controlling magnetic ordering in coupled nanomagnet arrays," New J. Phys. **1**, 16 (1999).
[71]I. Nekrashevich and D. Litvinov, "Ferromagnetic resonance in coupled magnetic nanostructured arrays," AIP Adv. **8**, 085002 (2018).
[72]J.-L. Déjardin, A. Franco, F. Vernay, and H. Kachkachi, "Ferromagnetic resonance of a two-dimensional array of nanomagnets: Effects of surface anisotropy and dipolar interactions," Phys. Rev. B **97**, 224407 (2018).
[73]P. K. Atanasova, S. A. Panayotova, E. V. Zemlyanaya, Yu. M. Shukrinov, and I. R. Rahmonov, "Numerical simulation of the stiff system of equations within the spintronic model," in *International Conference on Numerical Methods and Applications* (Springer, Cham, 2018), pp. 301–308.
[74]R. C. Hilborn, *Chaos and Nonlinear Dynamics: An Introduction for Scientists and Engineers*, 2nd ed. (Oxford University Press, London, 2008).
[75]S. K. Tolpygo, V. Bolkhovsky, S. Zarr, T. J. Weir, A. Wynn, A. L. Day, L. M. Johnson, and M. A. Gouker, "Properties of unshunted and resistively shunted Nb/AlO_x-Al/Nb Josephson junctions with critical current densities from 0.1 mA/μm^2 to 1 mA/μm^2," IEEE Trans. Appl. Supercond. **27**, 1100815 (2017).
[76]C. Manchein, R. M. da Silva, and M. W. Beims, "Proliferation of stability in phase and parameter spaces of nonlinear systems," Chaos **27**, 081101 (2017).
[77]R. Stoop, S. Martignoli, P. Benner, R. L. Stoop, and Y. Uwate, "Shrimps: Occurrence, scaling and relevance," Int. J. Bifurc. Chaos **22**, 1230032 (2012).
[78]C. Bonatto, J. C. Garreau, and J. A. C. Gallas, "Self-similarities in the frequency-amplitude space of a loss-modulated CO_2 laser," Phys. Rev. Lett. **95**, 143905 (2005).
[79]J. A. C. Gallas, "Structure of the parameter space of the Hénon map," Phys. Rev. Lett. **70**, 2714 (1993).
[80]Yu. M. Shukrinov, A. E. Botha, S. Yu. Medvedeva, M. R. Kolahachi, and A. Irie, "Structured chaos in a devil's staircase of the Josephson junction," Chaos **24**, 033115 (2014).
[81]G. Cicogna and L. Fronzoni, "Effects of parametric perturbations on the onset of chaos in the Josephson-junction model: Theory and analog experiments," Phys. Rev. A **42**, 1901 (1990).
[82]G. Ambika and J. Kurths, "Tipping in complex systems: Theory, methods and applications," Eur. Phys. J. Spec. Top. **230**, 3177 (2021).